

Low-Cost Photoacoustic System for Biomedical Applications

João Ferreira¹, Vânia Pinto^{1,2} , Tiago Matos^{1,2} , Susana O. Catarino^{1,2} , Graça Minas^{1,2} 
and Paulo Sousa^{1,2,*} 

¹Center for Micro Electromechanical Systems (CMEMS), University of Minho, Guimarães, 4800-058, Portugal

²LABELS — Associate Laboratory in Biotechnology and Bioengineering and Microelectromechanical Systems, University of Minho, Braga, 4710-057, Portugal

Keywords: Image Reconstruction, Photoacoustics, Scanning System.


Abstract: Recently, the field of photoacoustic (PA) imaging has garnered significant attention due to its ability to provide high-resolution images and real-time monitoring of biological tissues. However, PA systems have relied on expensive and complex laser sources and detection mechanisms, limiting their accessibility for widespread use in both clinical and research settings. So, this work aims to address these limitations by presenting the development of an alternative low-cost photoacoustic system, with an estimated cost of less than 700€, based on a Q-switched solid-state Nd:Ce:YAG nanosecond laser and a highly sensitive system for acoustic detection. PA data acquisition and image reconstruction were implemented and validated with pencil lead phantoms. The developed system shows a high potential to provide a low-cost tool that can be used in several biomedical applications.


1 INTRODUCTION


In recent years, photoacoustic (PA) has emerged as a new sensing technology that has been applied in the biomedical imaging field to obtain structural and functional information of cells and tissues non-invasively, providing highly specific molecular images. Furthermore, this imaging technology offers excellent spatial resolution, large imaging depth and high optical contrast (Beard, 2011; Erfanzadeh & Zhu, 2019; Zhu et al., 2024). It has been studied for tumour detection, epidermal melanin measurements, blood oxygenation monitoring, quantitative blood flow estimation, among others (Attia et al., 2019; John et al., 2023). Although its huge potential, the high cost of traditional PA systems and challenges in the miniaturization of the imaging components have limited their accessibility and widespread use in various fields, particularly in smaller laboratories and developing regions.


Typically, most of the commercial and research lab-made PA systems for biomedical applications use solid-state lasers to irradiate their targets, however these systems have been difficult to translate to clinical applications, due to their high cost and bulky size (Zhu et al., 2020). In recent years, low-cost solid-state laser, Laser Diodes (LDs) and light emitting diodes (LEDs) have emerged as alternative illumination sources, for the development of less expensive, compact and portable sensing and imaging systems (Zhong et al., 2018). Even though LEDs and LDs possess some disadvantages, such as low output energy, lack of spectral tuning capability, and long pulse widths, they are portable, affordable, and energy-efficient light sources (Singh & Xia, 2020).


In addition, the PA systems require ultrasonic detection methods that include piezoelectric transducers, micromachined ultrasound transducers (MUTs) (which can be divided into piezoelectric micromachined ultrasound transducer (pMUT),

^a  <https://orcid.org/0000-0003-3395-1251>

^b  <https://orcid.org/0000-0003-3826-6413>

^c  <https://orcid.org/0000-0002-8962-0710>

^d  <https://orcid.org/0000-0003-2460-0556>

^e  <https://orcid.org/0000-0003-2290-808X>

* Corresponding author.

capacitive micromachined ultrasound transducer (cMUT)) and optical transducers (Manwar et al., 2020). However, piezoelectric transducers are the most used transducers because of their well-established fabrication technology, reduced cost and dimensions and scalable sensitivity.

This work addresses this challenge by presenting the development of a novel and low-cost photoacoustic system that utilizes an affordable nanosecond tattoo removal laser as its light source with a unit price of ~€500 (compared with \$20–30 k for a regular system for PA testing and measurement) (Zhu et al., 2020; Zou et al., 2023), significantly reducing the typical investment required for such technology. Complementing the laser, a commercial lead zirconate titanate (PZT) transducer works as the acoustic receptor, while a low-cost logarithmic amplifier enhances the signal detection capabilities. To validate the performance of the developed system, experiments were conducted using pencil lead phantoms, enabling the assessment of the photoacoustic signal through a cost-effective electronic circuit. In addition, a scanning system and an image reconstruction system from the PA signals were developed. This innovative approach not only demonstrates the feasibility of creating an economical PA system but also opens new avenues for research and clinical applications that require high-quality imaging without prohibitive costs

2 PA SYSTEM'S DESIGN AND OPERATION

The PA effect is initiated when an pulsed electromagnetic wave targets the sample surface. Depending on the wavelength, the light penetrates to some depth in the target. Photon absorption and subsequent relaxation induce a rapid temperature rise, leading to the thermoelastic expansion of the absorbing target. This sudden pressure rise propagates as a sound wave, which then can be detected using an acoustic transducer. By detecting the pressure wave, one can localize their sources (i.e., where the light was absorbed) and obtain important functional and molecular information about the studied sample. More details about the theory and operational principles of PA detection are described in our previous work (Pinheiro et al., 2023; Pinheiro et al., 2024).

The developed PA system and the main operation principle are presented in Figure 1. An Q-switched solid-state Nd:Ce:YAG nanosecond laser (Ulat, B08G8S5YHF, China), commonly used for tattoo

removal, was used as light source. This equipment outputs 532 nm laser pulses with a pulse width of 8 ns and 40 mJ energy at a repetition rate of 10 Hz. An optical fiber was used to guide the light from the laser to the sample. A packaging assembly specifically engineered to support and align all the components, namely the excitation light and the acoustic transducer (PRYY+0398, PiMicos) was fabricated by 3D printing. For the scanning measurement system, two linear actuators (6V Push Rod, 30mm-128N, LA-T8-6-7-3085-128) connected in a 90-degree configuration were used to move in a controlled way the excitation light and the acoustic transducer together. The generated PA signals were detected by the acoustic transducer and amplified by the electronic circuit (AD8307 from Analog Devices). A STM microcontroller was used to control, store and acquire the PA signals which are sent to a PC where a python program was implemented to reconstruct the image. In the following sections, the main components of the developed PA system are described with more detail.

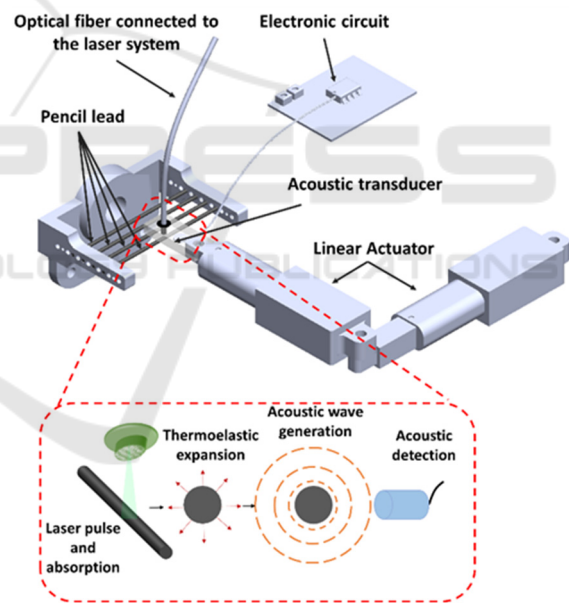


Figure 1: Schematic representation of the main components of the PA detection system.

2.1 Acoustic Transducer

The detection module of the PA system uses a PZT piezoelectric transducer with a 5 mm diameter and 250 μm thickness (PRYY+0398, PiMicos). The transducer electrical characterization was performed by measuring the S-parameters from 10 kHz to 20 MHz (without an impedance matching circuit), to determine the return loss (RL), which indicates the

reflected electrical power. The transducer shows RL peaks at 400 kHz and 8.8 MHz, corresponding to the radial and thickness resonance frequencies, respectively (Figure 2).

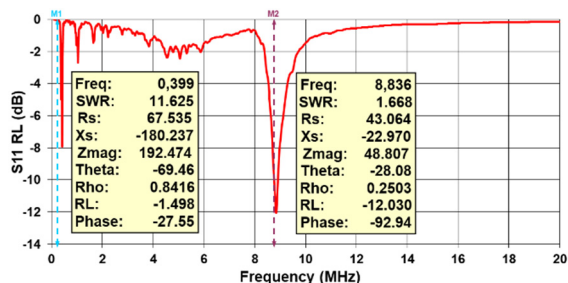


Figure 2: Return loss variation according to frequency for the transducer from 10 kHz to 20 MHz.

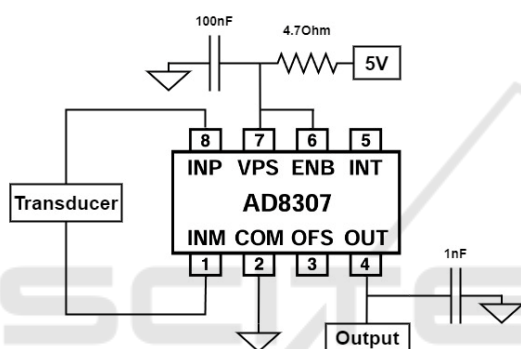


Figure 3: Electrical diagram of the circuit implemented in the amplifier.

2.2 AD8307 Amplifier

Typically, the PA signal induced by the nanosecond pulse laser has very low intensity, requiring an amplification circuit. For this purpose, the AD8307 integrated circuit was chosen. It is a complete 500 MHz monolithic demodulating logarithmic amplifier based on the progressive compression (successive detection) technique, providing a dynamic range of 92 dB to ± 3 dB law conformance and 88 dB to a tight ± 1 dB error bound at all frequencies up to 100 MHz. This logarithmic amplifier is widely used in radio frequency applications thanks to its vast list of advantages. The AD8307 operates in a wide frequency range, from DC up to 500 MHz, making it suitable for both low and high-frequency applications, and presents a wide dynamic range (-75 dBm to +15 dBm). It outputs a log-scale voltage directly proportional to the signal power, eliminating the need for extra circuits like rectifiers, filters, or log converters. Compared to traditional coupling circuits using standard operational amplifiers, the AD8307

provides an analogue output proportional to the input energy and frequency without needing multiple stages of amplification, attenuation, and additional components to handle radiofrequency (RF) signals and measure power over a wide range. In addition, it requires minimal adjacent electronic components, making it easy to integrate in pre-existent circuits.

The electrical diagram of the implemented circuit is presented in Figure 3. A low-pass filter (12.7 kHz cutoff frequency) was added to the amplifier output to reduce high-frequency noise.

2.3 Signal Acquisition

The PA signal acquired by the amplification circuit was initially displayed in an oscilloscope. After validation, a signal acquisition system was implemented using an algorithm to process the data. For this purpose, an STM32H503RB development board was used. This board was chosen due to its high clock frequency, 250 MHz, which enables a very high rate of data acquisition, thus providing a more detailed data acquisition. This is essential for the developed PA system since the duration of the obtained signal is approximately 200 μ s, as it can be seen in the Figure 4.



Figure 4: Photoacoustic signal recorded by an oscilloscope.

After connecting the board to the amplification circuit so that its output is connected to the boards' analog to digital converter (ADC), and ensuring a common ground between the two, the signal can be acquired. It should be noted that the ADC has a maximum resolution of 12 bits, meaning the highest value it can return is $2^{12} = 4095$. Furthermore, given that the maximum supported voltage by the ADC is 3.3 V, using a simple proportion, any value transmitted by the ADC can be converted into a voltage value using the following equation:

$$\text{Voltage} = (\text{ADC value} \times 3.3) / 4095 \quad (1)$$

Regarding the implementation of the data acquisition, firstly an array was created with its size corresponding to the number of samples to be acquired. After this, the board's ADC is initialized and waits to receive a value greater than 2000 to start the acquisition. This condition was implemented to ensure that only signals of interest are acquired; without it, any interference, could trigger the beginning of the process. The electromagnetic noise caused by the laser firing is used as a trigger signal to synchronize the STM with the photoacoustic system. Once this condition is met, the acquisition begins, and the array is filled. Once full, its values are transmitted via the serial port and the array is restarted with its values set to 0, thus allowing to restart the process, according to the following commands:

```
#define array_size 2000
Void read_adc_array(){
...
HAL_ADC_Start(&hadc1);
while(val[0]<2000){
    ...
}
for(int i=0; i<array_size; i++){
    val[i] =
        (int16_t)HAL_ADC_GetValue(&hadc1);
}
HAL_ADC_Stop(&hadc1);
for (int i=0; i<array_size;i++){
    ...
    HAL_UART_Transmit(&huart3,
uint8_t*)tx, strlen(tx), 200);
    val[i]=0;
}
}
```

Since the data is being transmitted via serial port, the next step is saving it to the computer. In a first stage, the PUTTY software (v0.82) was used to receive and store the received values, enabling the creation of the Figure 5 plot.

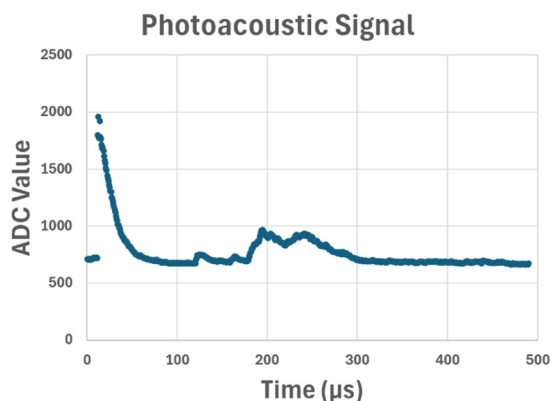


Figure 5: ADC values (a.u.), related to the generated photoacoustic signal, acquired by the microcontroller over time (μs).

2.4 Motor Control

Having confirmed the viability of the data acquisition using the microcontroller, it was also chosen for another critical task: to enable the imaging of a pre-selected region of interest (ROI). To meet this requirement, two motors were employed, each responsible for moving the scanning system across an (X,Y) plane. The selected motors are linear actuators with a maximum boom of 3 cm, operating at a voltage of 3.3 V. This allows for the coverage of a 9 cm² total area, enough to analyse the entire ROI. Moreover, their power can be directly supplied by the microcontroller, as well as its control algorithm, thus simplifying the project by not having to rely on an external motor driver.

To control the actuators, it was first necessary to determine their velocity, to calculate how long they need to be activated to extend a given distance. Through multiple tests, it was found that the actuators take approximately 14.2 seconds to reach their maximum length. Thus, it was calculated that to move 1 mm, the active time required is 473.3 ms.

Finally, each motor is connected to two General Purpose Input/Output (GPIO) pins capable of providing voltage values between 0-3.3 V. By toggling these pins, the direction of the movement can be changed, as well as stopping their motion:

```
Void move_x_axis(){
uint32_t startTime= HAL_GetTick();
uint32_t elapsedTime = 0;
while (elapsedTime < 473){
    HAL_GPIO_WritePin(GPIOC,
GPIO_PIN10, GPIO_PIN_RESET);
    HAL_GPIO_WritePin(GPIOC,
GPIO_PIN_12, GPIO_PIN_SET);
    elapsedTime = HAL_GetTick() -
startTime;
}
}
```

The last step is to ensure that the motors are moving in a pattern that allows them to cover a predetermined area. For this, a loop was implemented to control their movement in a grid-like motion:

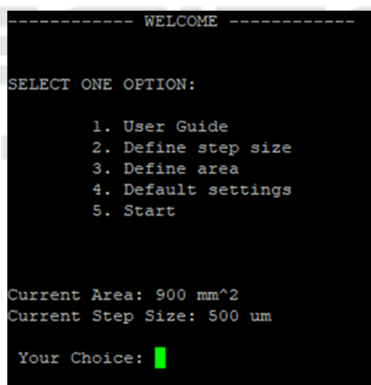
```
Void grid_movement(){
for(int i=0;i<10;i++){
    for(int j=0;j<10;j++){
        move_y();
        read_adc_array();
    }
    home_y();
    move_x();
}
home_x();
home_y();
}
```

2.5 User Interface

A command-line user interface has been developed to facilitate an efficient and intuitive interaction with the system. By default, the system is configured to analyse the maximum area with a resolution of 500 μm per step. However, the interface provides several configurable options to better align the system's operation with specific application requirements.

The available features include: a user guide to explain how the system works, Step Size Adjustment that enables modification of the resolution of the step size and analysis area configuration that allows customization of the area to be analysed, optimizing the process for various applications (Figure 6).

Due to the resource limitations of the STM32 platform, all interactions are conducted through the command-line interface, as implementing a graphical user interface (GUI) would be impractical. Parameters defined by the user via this interface are automatically transferred to the accompanying Python script running on a connected computer. This ensures that the generated graphical output adheres to the specified parameters.



```

----- WELCOME -----
SELECT ONE OPTION:
  1. User Guide
  2. Define step size
  3. Define area
  4. Default settings
  5. Start

Current Area: 900 mm^2
Current Step Size: 500 um

Your Choice: █

```

Figure 6: Example of the User Interface.

2.6 Data Analysis

Having successfully acquired the required data using the microcontroller and established a method for controlling the system's position, the final step involves implementing an algorithm to analyse the data and present it in a clear and user-friendly interface. To achieve that, a Python script was developed to read the serial port of the computer, save the received data locally on the machine and do the necessary processing. Firstly, some parameters needed to be set, namely the port being used, its baud rate and the amount of data points being received. The

next step is to initialize the connection and read the data:

```

try:
    ser = serial.Serial(COM_PORT, BAUD_RATE)
    print(f"Connected to {COM_PORT} at {BAUD_RATE} baud.")
except serial.SerialException as e:
    print(f"Error connecting to {COM_PORT}: {e}")
    exit()

```

After a successful connection, the data is stored in an array which, when filled with the total points, is saved in a .txt file.

```

while len(data) < TOTAL_POINTS:
    line = ser.readline().decode('utf-8', errors='ignore').strip()
    file.write(line + "\n") # Save the line to the file

```

Now that all the data has been received, some conditioning needs to be done so that it reflects real-world conditions. For now, the array is storing all the values in the order they were transmitted but, since every measurement consists of 2000 data points, the main array needs to be subdivided into smaller ones with 2000 entries each. After this subdivision has taken place, the next step is to focus on the entries which contain the photoacoustic signal. As seen on Figure 5, the signal starts roughly 150 μs after the electromagnetic discharge produced by the laser and has a duration of 150-200 μs . To only interpret the data points stored in those positions, the maximum value of the array needs to be found:

```

def find_max_per_chunk(data, chunk_size):
    max_values = []
    for i in range(0, len(data), chunk_size):
        chunk = data[i:i + chunk_size]
        max_values.append(max(chunk))
    return max_values

```

Knowing in which position the electromagnetic spike occurs, the next step is to trim the initial array that contains 2000 entries into smaller ones that only contain the values present from 150 μs to 300 μs . Since we know that each entry occurs at intervals of 0.7 μs , we know that is going to be roughly taking place around sample number 200-400.

```
def extract_values_after_max(data,
    chunk_size, offset_start, offset_end):
    extracted_values = []
    for i in range(0, len(data),
        chunk_size):
        chunk = data[i:i +
            chunk_size]
        max_idx = chunk.index(max(chunk
            start_idx = max_idx +
            offset_start
            end_idx = max_idx + offset_end
            if start_idx < len(chunk):
                extracted_values.append(chu
                    nk[start_idx:min(end_idx, len(chunk))])
            return extracted_values

offset_start = 200
offset_end = 400

values_after_max =
    extract_values_after_max(data,
        chunk_size, offset_start, offset_end)
```

The last step is to find the maximum value inside these new chunks of data, which will tell us if there is any PA response and represent it in a cartesian graph that will allow the data visualization. The values are presented in a grayscale where the minimum value is represented by the color black and the maximum by the color white.

3 EXPERIMENTAL SETUP FOR THE PA SYSTEM TEST

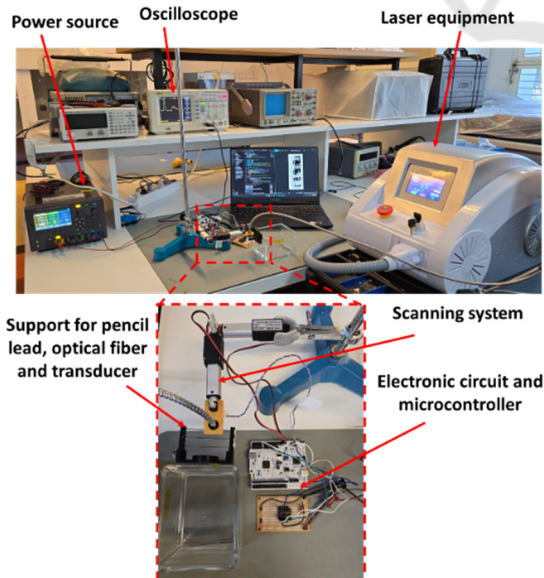


Figure 7: Setup for the experimental tests.

The experimental tests were conducted with the setup shown in Figure 7, which comprises the power source used to supply the amplifier circuit and the microcontroller; the amplification circuit and the STM32 H503RB; the support for sample, optical fiber and transducer and the laser equipment, responsible for the light excitation.

To validate the PA system, several pencil lead phantoms were employed. A matrix of pencil lead (Graphite HB 0.7 mm), arranged in 4 rows with a spacing of about 5 mm, was fabricated using 3D printed plastic holders. Using this solution allows us to keep the low cost of the tests and ensure reproducibility. In addition, the high content of carbon in the pencil lead allows obtaining strong photoacoustic signals (Zou et al., 2023).

4 RESULTS AND DISCUSSION

A first test with a single pencil lead was performed to observe the maximum peak output and evaluate the PA signal (Figure 8).

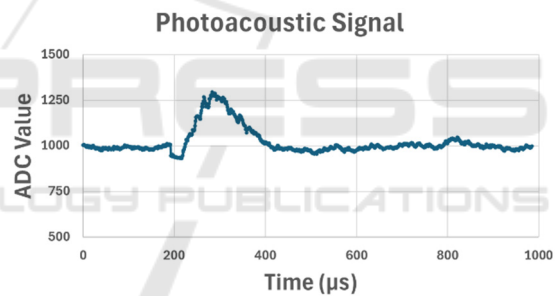


Figure 8: ADC values (a.u.), related to the generated photoacoustic signal, after processing, as a function of time (µs).

As can be seen, a constant signal was received by the ADC with an approximate value of 1000, which equates to 0.805 V (-57.8 dB). When the PA response is triggered, a spike can be seen, reaching the value of 1300, which represents 1.05 V (-48 dB), an increase of 0.245 V over the constant value generated by the circuit. After the previous validation, a test with all the modules was performed. A scanning area of 200 mm² was defined for the test, corresponding to an X distance of 5 mm and an Y distance of 40 mm, allowing measuring the PA response of four pencil lead lines. One acquisition was made at each coordinate, which was then processed to PA image reconstruction. The schematic representation of the main steps for data acquisition, processing and reconstruction are presented in Figure 9.

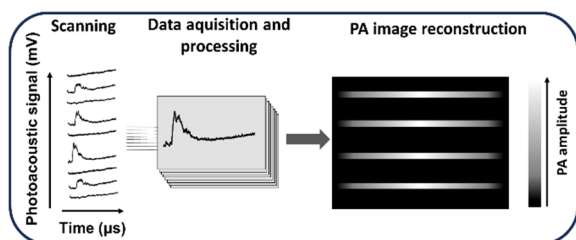


Figure 9: Schematic representation of the main steps of PA image reconstruction.

The reconstructed final image, in Figure 10, shows the capability of the developed system to map the spatial distribution of all four targets (pencil lead), where the color shifts from black to white. Although it is possible to identify four distinct regions, coinciding with the position of the graphite, the lateral resolution presents some limitations in accurately discriminating the separation between them. This limitation can be improved by reducing the laser focal point to decrease the irradiation area and increase the potential of the developed system.

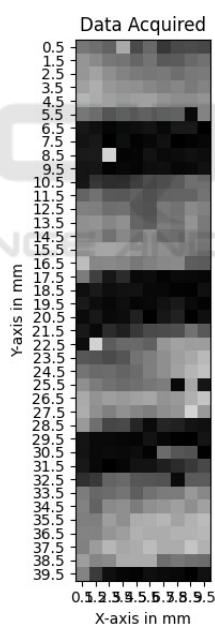


Figure 10: 2D Image reconstructed from the PA signals of the four pencil leads.

5 BIOMEDICAL APPLICATIONS OF PHOTOACOUSTIC SYSTEMS

The developed PA imaging system can be used in several biomedical applications, namely in

microfluidic lab-on-a-chip devices to monitor haemoglobin quantities (Pinheiro et al., 2024), or in organ-on-a-chip devices to provide, for example, a mapping of the spatial distribution of drugs (such as the antitumor drug doxorubicin) within cells or tissues, in a continuous way. The real-time monitoring of the cell's response to new compounds allows has potential to accelerate the clinical translation of new vaccines and drugs. In addition, it can have a significant impact on the understanding of the efficiency of new drugs, which potential to lower the amount of drugs needed for the treatment of diseases, decreasing their side effects and ensuring better population ageing conditions.

6 CONCLUSIONS

This paper presents a detailed characterization of the development and validation of a low-cost photoacoustic system, with high potential for future application in biomedical devices.

Using pencil lead phantoms, the developed system was able to detect the PA signals and reconstruct the corresponding image with good accuracy.

Future improvements are needed to increase the lateral resolution of the system, namely with the use of optical lenses to reduce the area of the incident light.

ACKNOWLEDGEMENTS

This work has been supported by the project DrugSENS (2022.02165.PTDC) (<https://doi.org/10.54499/2022.02165.PTDC>), through national funds (OE), within the scope of the Scientific Research and Technological Development Projects (IC&DT) program in all scientific domains (PTDC), through the Foundation for Science and Technology, I.P. (FCT, I.P). The authors also acknowledge the partial financial support within the R&D Unit Project Scope: UIDB/04436/2020. Susana Catarino, Paulo Sousa and Vânia Pinto thank FCT for their contracts funding provided through 2020.00215.CEECIND (DOI: <https://doi.org/10.54499/2020.00215.CEECIND/CP1600/CT0009>), 2021.01086.CEECIND (<https://doi.org/10.54499/2021.01086.CEECIND/CP1664/CT0008>) and 2021.01087.CEECIND (<https://doi.org/10.54499/2021.01087.CEECIND/CP1664/CT0020>), respectively.

REFERENCES

- Attia, A. B. E., Balasundaram, G., Moothanchery, M., Dinish, U. S., Bi, R., Ntziachristos, V., & Olivo, M. (2019). A review of clinical photoacoustic imaging: Current and future trends. *Photoacoustics*, *16*, 100144.
- Beard, P. (2011). Biomedical photoacoustic imaging. *Interface focus*, *1*(4), 602-631.
- Erfanzadeh, M., & Zhu, Q. (2019). Photoacoustic imaging with low-cost sources; a review. *Photoacoustics*, *14*, 1.
- John, S., Hester, S., Basij, M., Paul, A., Xavierselvan, M., Mehrmohammadi, M., & Mallidi, S. (2023). Niche preclinical and clinical applications of photoacoustic imaging with endogenous contrast. *Photoacoustics*, 100533.
- Singh, M. K. A., & Xia, W. (2020). Portable and affordable light source-based photoacoustic tomography. *Sensors* *20*(21), 6173.
- Manwar, R., Kratkiewicz, K., & Avanaki, K. (2020). Overview of ultrasound detection technologies for photoacoustic imaging. *Micromachines*, *11*(7), 692.
- Pinheiro, B. R., Dinis, H. D., Catarino, S. O., Pinto, V. C., Sousa, P. J., & Minas, G. (2023, June). Experimental Characterization of a Piezoelectric Transducer for Integration into a Photoacoustic System. In *2023 IEEE 7th Portuguese Meeting on Bioengineering (ENBENG)* (pp. 84-87). IEEE.
- Pinheiro, B., Pinto, V., Dinis, H., Belsley, M., Catarino, S., Minas, G., & Sousa, P. (2024). Development of a Photoacoustic Acquisition System and their Proof-of-Concept for Hemoglobin Detection. *Heliyon*.
- Zhong, H., Duan, T., Lan, H., Zhou, M., & Gao, F. (2018). Review of low-cost photoacoustic sensing and imaging based on laser diode and light-emitting diode. *Sensors*, *18*(7), 2264.
- Zhu, X., Menozzi, L., Cho, S. W., & Yao, J. (2024). High speed innovations in photoacoustic microscopy. *npj Imaging*, *2*(1), 46.
- Zhu, Y., Feng, T., Cheng, Q., Wang, X., Du, S., Sato, N., ... & Kuniyil Ajith Singh, M. (2020). Towards clinical translation of LED-based photoacoustic imaging: a review. *Sensors*, *20*(9), 2484.
- Zou, E., Fang, C., & Song, D. (2023). A Low-Cost Handheld Photoacoustic (PA) Probe for Rapid and Non-Destructive Detection of Watermelon Ripeness. *IEEE Sensors Journal*.